Comparison of Vapor Formation of Water at the Solid/Water Interface to Colloidal Solutions Using Optically Excited Gold Nanostructures

Susil Baral,[†] Andrew J. Green,[†] Maksim Y. Livshits,[†] Alexander O. Govorov,[‡] and Hugh H. Richardson[†,*]

[†]Department of Chemistry and Biochemistry, Ohio University, Athens, Ohio 45701, United States and [‡]Department of Physics and Astronomy, Ohio University, Athens, Ohio 45701, United States

ABSTRACT The phase transformation properties of liquid water to vapor is characterized by optical excitation of the lithographically fabricated single gold nanowrenches and contrasted to the phase transformation properties of gold nanoparticles located and optically excited in a bulk solution system [two and three dimensions]. The 532 nm continuous wave excitation of a single gold nanowrench results in superheating of the water to the spinodal decomposition temperature of 580 ± 20 K with bubble formation below the spinodal decomposition temperature being a rare event. Between the spinodal decomposition temperature and the boiling point liquid water is trapped into a metastable state because a barrier to vapor nucleation exists that must be overcome before the thermodynamically stable state is realized. The phase transformation for an optically heated single gold nanowrench is different from the phase transformation of optically excited colloidal gold nanoparticles solution where collective heating effects dominates and leads to the boiling of the solution exactly at the boiling point. In the solution case, the optically excited ensemble of nanoparticles collectively raises the ambient temperature of water to the boiling point where liquid is converted into vapor. The striking difference in the boiling properties of the single gold nanowrench and the nanoparticle solution system can be explained in terms of the vapor-nucleation mechanism, the volume of the overheated liquid, and the collective heating effect. The interpretation of the observed regimes of heating and vaporization is consistent with our theoretical modeling. In particular, we explain with our theory why the boiling with the collective heating in a solution requires 3 orders of magnitude less intensity compared to the case of optically driven single nanowrench.

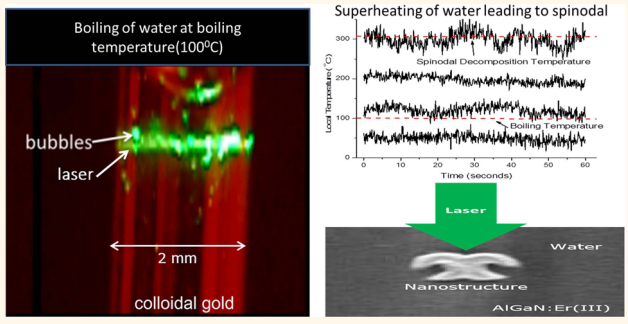

KEYWORDS: heat generation · gold nanowrenches · spinodal decomposition temperature · vapor nucleation

The number of solar thermal energy power plants around the world is increasing as solar thermal energy conversion becomes more efficient and replacing power stations that use fossil fuels with a pollution free sustainable source of energy becomes more feasible.[1] Understanding the mechanism of converting light to heat using heterogeneous supports is important in improving the efficiency and alternately reducing production costs of megawatt solar thermal power plants. Recently, Halas and co-workers have published a series of papers on solar thermal energy conversion using nanostructures as broadband light-harvesting agents.[2−4] A mechanism of steam generation using broadband light absorbing nanoparticles is postulated where nanoparticle bubble complexes reach the surface of the liquid and release steam. This process occurs with a large temperature difference between the optical heated nanoparticle bubble complex and the ambient temperature of the liquid.

Classical nucleation theory reveals that bubble nucleation from nanometer-sized structures should not occur at temperatures closed to the boiling point but at large superheated temperatures.[5] Flat surfaces or surfaces with nanometer or micrometer posts do not nucleate vapor until the temperature reaches the kinetic limit for heterogeneous nucleation. This limit occurs

* Address correspondence to richards@helios.phy.ohiou.edu.

Received for review October 9, 2013 and accepted January 29, 2014.

Published online January 29, 2014
10.1021/nn405267r

at ~0.89 of the critical temperature where the vapor nucleation rate is given by the homogeneous nucleation rate. In contrast, cavities in surfaces are capable of trapping vapor when submerged with liquid. The trapped vapor is capable of nucleating vapor with the magnitude of superheating related to the size of the cavity. Larger micrometer-sized cavities nucleate vapor at a lower superheated temperature than smaller nanometer-sized cavities. These results have been recently experimentally verified using nanometer to micrometer-sized posts and cavities fabricated with e-beam lithography.[6]

We have previously shown that a colloidal solution of gold nanoparticles excited with light raises the ambient temperature of the liquid through collective heating effects if the particle density leads to a particle spacing where the heat signature from individual particles overlap.[7] This result is supported by theory where enhanced temperatures are observed for collective excitation of nanoparticle solutions.[8,9] This mechanism is in contrast to a mechanism recently proposed where a large temperature difference between the nanoparticle and the supporting fluid is postulated.[2−4] Our mechanism of steam generation involves a process where the ambient temperature of the liquid is raised by collective heating effects to the saturation temperature where bubble formation occurs, not at the surface of the nanoparticles but at heterogeneous nucleation sites within the liquid. In this mechanism, a large number of nanoparticles are excited simultaneously and release heat to the surrounding fluid raising the ambient temperature of the fluid to the boiling point where bubbles nucleate heterogeneously.[7−9] In another experiment,[10] the vapor bubbles were generated in water and biological matrixes using micrometer-size nanoparticle clusters and again the collective-heating theory provided reasonable estimates for the temperature increase. More examples of the collective heating mechanism are found in papers on melting of DNA-assembled gold nanoparticle clusters,[11] nanoparticle arrays[12] and melting of ice matrix.[13]

Recently, we have shown that individual gold nanodots at a solid/liquid interface optically excited using continuous wave excitation do not preferentially induce bubble formation at the boiling point but superheat the liquid around the nanodot.[14] We proposed that superheating of the liquid in close proximity of the nanodot occurs because there is a barrier to vapor formation that traps the liquid in a metastable state. This barrier exists for temperatures as high as the spinodal decomposition temperature where the liquid is no longer metastable but spontaneously decomposes into the thermodynamic stable states at that temperature. This picture is in agreement with classical nucleation theory.[5] In this paper we explore the relationship between the superheated liquid and bubble formation for a single optically excited nanostructure at the gold/water interface. The nanostructure we interrogate is a nanowrench having both post and cavity structure. We contrast these properties with vapor formation in a colloidal solution of optically excited gold nanoparticles. We find that bubble formation for a single nanostructure at a solid/water interface is an inherently a low probability event with superheating of the liquid to the spinodal decomposition temperature as the norm. In contrast to this, a colloidal solution of gold nanoparticles optically excited form steam bubbles at the boiling point. The ambient liquid temperature is raised to the boiling point by collective heating effects and boiling occurs within the solution and not necessarily at the surface of the nanoparticle. This mechanism is consistent with classical nucleation theory[5] where boiling in a bulk liquid starts at a nucleation center (a small air bubble or another object). Nucleation centers diffuse in a liquid and sometimes enter the superheated area. Therefore, the probability and frequency of appearance of vapor bubbles strongly depend on the volume of the superheated water. In the case of the solution experiments, this superheated-water volume is orders of magnitude larger than that in the single nanowrench experiment. This extreme difference in heated volumes leads to the behavior where vapor bubble creation in the solution case is a frequent event, whereas in the single nanostructure case, bubbles happen to be very rare events.

RESULTS

Temperature Changes and Phase Transformation with Gold Nanowrenches. Figure 1 shows the SEM image of the lithographically fabricated gold nanowrenches. The nominal length and width of the nanowrench is 700 and 400 nm, respectively, with a height of 65 nm. The nanowrenches were fabricated in arrays having spacing between nanowrenches of 3000 nm. The beam width of the excitation laser (fwhm) is ~800 nm ensuring that only a single gold nanowrench was excited.

Figure 2 shows the local temperature change of the gold nanowrench immersed in water as a function of excitation laser intensity. Different colored data points represent data collected on different days. This data can be divided into two different regions where the properties are quite different. At low laser intensities a linear region is observed where the local temperature

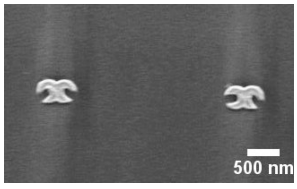

Figure 1. SEM image of the lithographically fabricated gold nanowrench with standard length, width, and height of 700, 400, and 65 nm, respectively.

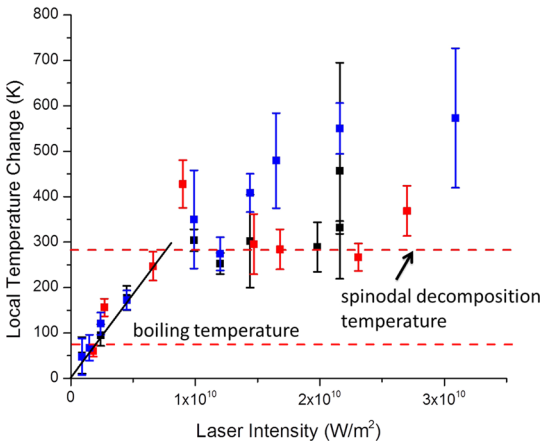

Figure 2. A plot of a local temperature change in K as a function of laser intensity in W/m^2. The temperature increased linearly with increasing laser intensity until reaching the value around ΔT of 280 K, where fluctuations in temperature were seen with increasing laser intensity.

varies linearly with laser intensity. The measured temperature is scaled with a factor of 10.2 to account for the difference between the temperature at the nanowrench and the temperature averaged across the optical collection volume.[14−16] The linear temperature region goes beyond the boiling point of water (373 K) and extends to the spinodal decomposition temperature of water at 580 K. At the spinodal decomposition temperature of water, the characteristics of temperature with laser intensity change dramatically. In the second region, the temperature does not vary linearly with laser intensity but multiple temperatures are observed at each laser intensity. The temperature variation in the second region was probed by taking temperature time traces at constant laser intensity.

Figure 3 shows temperature time traces for different laser intensities. At low laser intensity, the average local temperature is below the boiling point of water. In temperature trace A, a single nanowrench was heated with a laser intensity of 1.5×10^9 W/m^2 for a time period of 60 s. The photoluminescence spectrum at each time interval is converted into temperature. Background temperature traces are collected for each laser intensity and subtracted from the sampled temperature trace to give the difference temperature trace shown in Figure 3. The number of counts in the photoluminescence spectrum scales with laser intensity so a lower temperature variation is expected at higher laser intensities. Temperature traces B (laser intensity 2.4×10^9 W/m^2) and C (laser intensity 4.5×10^9 W/m^2) are at an average temperature above the boiling point of water but below the spinodal decomposition temperature. The temperature variation in the trace is diminishing with higher laser intensity as expected. This behavior changes in temperature trace D (laser intensity 1.2×10^{10} W/m^2) taken at the spinodal decomposition temperature of 580 $\pm$ 20 K.

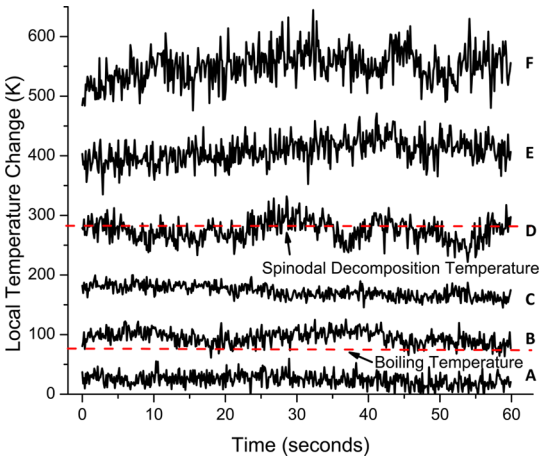

Figure 3. Temperature−time spectra of a single nanowrench at different laser intensities. The nanowrench was heated with different laser intensities (A, 1.50×10^9; B, 2.40×10^9; C, 4.50×10^9; D, 1.20×10^{10}; E, 1.44×10^{10}; F, 2.16×10^{10} W/m^2) for a time period of 60 s. The red dashed line designates the boiling and spinodal decomposition temperature of water.

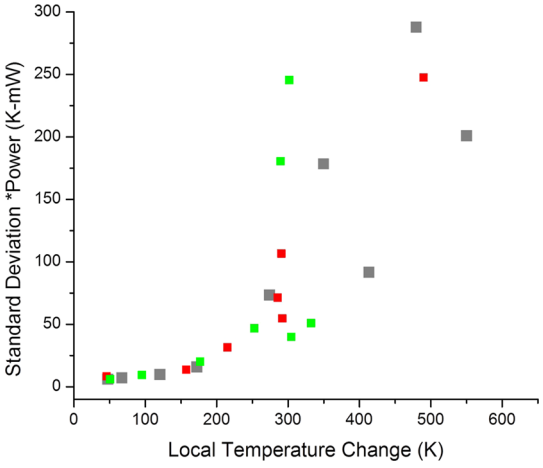

Figure 4. A plot of standard deviation multiplied by the laser intensity as a function of the local temperature change. The standard deviation is determined from temperature−time spectra where representative spectra are shown in Figure 3.

The variation in temperature has both high and low frequency components. Above the spinodal decomposition temperature, the temperature variation increased with temperature (traces E and F, laser intensity 1.44×10^{10} and 2.16×10^{10} W/m^2, respectively). The variation in temperature as a function of temperature can be characterized by taking the standard deviation of the temperature trace from the average temperature and multiply by the laser intensity. If the system is behaved as expected, then such a plot should show no variation with temperature.

Figure 4 shows the standard deviation multiplied by the laser intensity as a function of the local temperature change. A flat line is observed at low temperature that slope increases to the spinodal decomposition

temperature where a dramatic break in the trend is observed. At temperatures at and above the spinodal decomposition temperature ($\Delta T = 280 \pm 20$ K), wild fluctuations in temperature are observed that increase the standard deviation significantly. To probe the temperature structure properties of the water near the nanowrench, both the lossless scattering of the excitation laser and photoluminescence from the thermal sensor film were collected simultaneously.

The overlaid temperature and scattering time traces are shown in Figure 5 for temperatures between the boiling and spinodal decomposition points and for temperatures much above the spinodal decomposition temperature. The data, shown in red, is scattering collected back through the microscope objective at the excitation wavelength. The data, shown in black, is the temperature trace converted from the photoluminescence spectrum and scaled to yield the local temperature. The data shown in Figure 5A is taken at a laser intensity of 2.4×10^9 W/m^2. The temperature of the nanowreches for this laser intensity is near the boiling point of the water and both the temperature and scattering traces have similar properties. In contrast to this behavior, for data collected much above the spinodal decomposition temperature (shown in Figure 5B, laser intensity 3×10^{10} W/m^2), the temperature and scattering profiles move in opposite directions with an increase in temperature corresponding to a decrease in laser scattering.

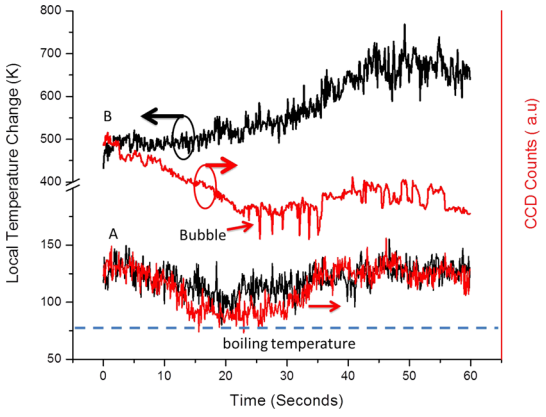

Figure 5. Temperature–time spectra (shown in black) overlaid on laser scattering spectra (shown in red) at laser intensity of 2.4×10^9 and 3.10×10^{10} W/m^2. Evidence of bubble formation is revealed as dips in the laser scattering spectra. Bubbles formed at temperatures between the boiling and spinodal decomposition temperature are rare but long-lived, while bubble formation for temperatures above the spinodal decomposition temperature are shorter lived but happen frequently.

Figure 6 shows three successive frames each 0.04 s apart from a movie (Supporting Information) showing water boiling after laser excitation of a colloidal solution containing 13 nm diameter gold nanoparticles. The solution is excited at 532 nm with 1.0 W laser power. The laser spot size is 0.3 mm yielding a laser intensity of 1.8×10^7 W/m^2. The green line in the figure is the 532 nm laser. Panel A is just before boiling, while panels B and C show spontaneous boiling of the solution with a large bubble forming within the capillary tube.

Figure 7 shows the temperature inside the capillary tube at distances away from the laser excitation area when a gold nanoparticle colloidal solution, concentration of 9×10^{10} particles/cm^3 and 40 nm diameter, is excited at 532 nm. The laser power is changed from 0 to 500 mW. The temperature within the laser excitation (0 mm distance) is impossible to probe with the thermocouple and must be extrapolated from the exponential fit of the thermal data away from the center of the laser excitation area.

Convection within the liquid is probed by measuring the temperature distribution within the optically stimulated liquid as the laser is moved from the bottom to top of a liquid sample cell (see the Materials and Methods section). The temperature profiles within the liquid at different laser positions are shown in Figure 8C. The color coded arrows show the position of the laser excitation. When the sample is excited in the middle of the sample cell (laser position 3, red data), the temperature in the liquid 2 mm above the laser spot is higher than the temperature at the laser spot indicating movement of the hot liquid. In the diagram shown at the far left of the Figure 8A, the laser is excited at positions labeled 1 through 5 and is color coded to the temperature profiles shown in Figure 8C. Figure 8B diagrams the general movement of the hot liquid within the sample cell.

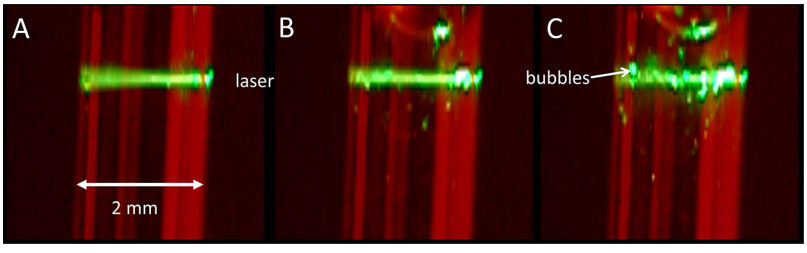

Figure 6. Three successive frames each 0.04 s apart from a movie (Supporting Information) showing water boiling after laser excitation of a colloidal solution containing 13 nm diameter gold nanoparticles. The solution is excited at 532 nm with a laser intensity of 1.8×10^7 W/m^2.

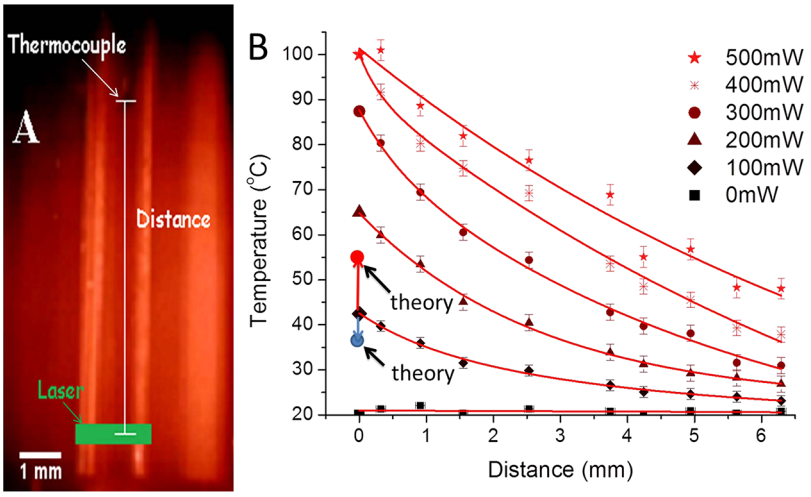

Figure 7. Temperature profiles of the liquid within the capillary tube (2 mm diameter) at distances away from the laser excitation area when a gold nanoparticle colloidal solution, with concentration of 9×10^{10} particles/cm^3 and 40 nm diameter, is excited at 532 nm. The laser intensity is changed from 0 to 9×10^6 W/m^2. We also include two theoretical points calculated by eqs 1 and 2 for the 100 mW excitation.

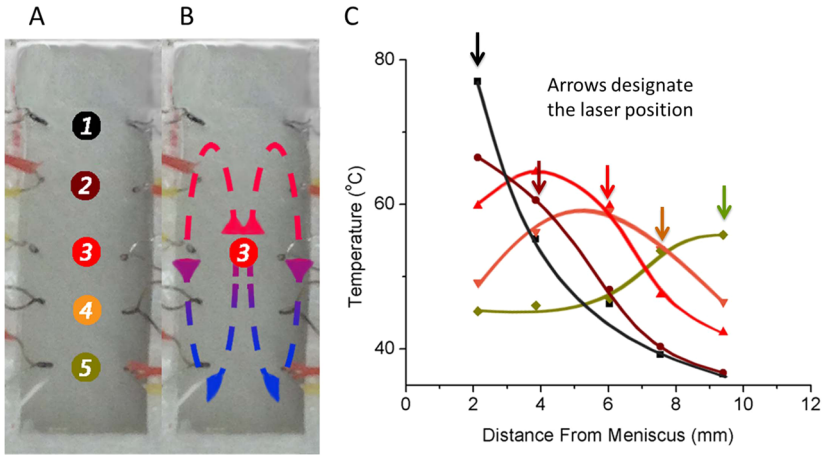

Figure 8. Panels A is a picture of the sample cell showing the position of laser excitation and the thermocouples used to measure the temperature within the sample cell. Panels B is a diagram showing the expected rise in hot liquid when excited at laser position 3. The temperature profiles within the liquid at different laser positions are shown in panel C. The color coded arrows show the position of the laser excitation. When the sample is excited in the middle of the sample cell (laser position 3, red data), the temperature in the liquid 2 mm above the laser spot is higher than the temperature at the laser spot indicating movement of the hot liquid.

DISCUSSION

Metastability of Superheated Water. It is possible to heat water well above the boiling point (superheat) because a free energy barrier exists between the metastable state (superheated water) and the global stable state (gas). Superheated water will remain as a liquid for a period of time but will ultimately, given enough time, transition to the globally minimum free energy state. The limit of stability, the point where small perturbations decrease the free energy of the system, is called the spinodal. If the temperature of metastable water at ambient pressure is raised to the spinodal decomposition temperature (594 ± 17 K),[14] the liquid water will spontaneously collapse into mixed phases of higher and lower density.[17] Unlike bubble nucleation, spinodal decomposition is not an activated process and results in a phase transition that has different characteristics. First, there is no free energy barrier for spinodal decomposition and the transition occurs spontaneously compared to bubble nucleation that is a stochastic process. Second, the superheated water at the spinodal decomposition temperature (SDT) spontaneously collapses with a large increase in pressure corresponding to the saturation pressure at the spinodal temperature (92 bar).

Phase Transformation Characteristics for Two-Dimensional Vapor Nucleation. Figure 2 shows the local temperature change as a function of laser intensity. At low laser intensity, the local temperature change is linear with laser intensity. Also, the standard error of the measurement decreases with laser intensity because the Er^{3+} photoluminescence increases with increasing laser

intensity. These characteristics change dramatically at a local temperature change of 280 ± 20 K where the temperature no longer increases linearly and the standard error of the measurement decreases with increasing laser intensity. In this region the temperature levels off and fluctuates at and above the spinodal decomposition temperature.

The time dependence in the local temperature change was monitored by collecting time traces of the local temperature change at temperatures below and above the spinodal decomposition temperature. These time traces are shown in Figure 3. Below the spinodal decomposition temperature, the standard deviation in the traces reduces with laser intensity as expected, but above the SDT, the standard deviation increases. The decrease in the standard deviation is expected to be linearly proportional to the laser intensity. A plot of standard deviation multiplied by the laser intensity as a function of local temperature change is shown in Figure 4. A clear demarcation in the characteristics for the standard deviation is observed at a temperature change of 280 K. This demarcation is consistent with the assignment that the SDT occurs at a temperature change of 280 K.

Vapor nucleation from the liquid is an activated process. Cavities of dissolved gases within the liquid greatly increase the nucleation rate but it is possible to superheat liquid water droplets (~0.5 mm) within a host liquid to nearly 280 °C by careful elimination of dissolved gases and solid impurities.[18] We were able to observed vapor bubble nucleation below the spinodal decomposition temperature but it is a rare event. Figure 5 shows the local temperature change and laser scattering of bubble nucleation events. The traces shown in Figure 5A reveal that the temperature and laser scattering track each other at temperatures below the spinodal decomposition temperature and that the bubble is long-lived (25 s). The traces above the spinodal decomposition temperature, shown in Figure 5B, have very different behavior than the temperature and scattering traces below the spinodal decomposition temperature. The temperature and laser scattering profiles no longer track each other and the bubble lifetime is greatly reduced.

Phase Transformation Characteristics for Three-Dimensional Vapor Nucleation. A gold nanoparticle colloidal solution, 13 nm diameter, is excited at 532 nm with 1.0 W laser power. The laser spot size is 0.3 mm yielding a laser intensity of 1.8×10^7 W/m^2. Figure 6 shows three consecutive frames, each 0.04 s apart, taken from a movie of water boiling when excited with laser light (see Supporting Information). The green line in the figure is the 532 nm laser. Panel A is just before boiling, while panels B and C show spontaneous boiling of the solution with a large bubble forming within the capillary tube.

Figure 7 shows the temperature inside the capillary tube at distances away from the laser excitation area for a 40 nm diameter gold colloidal solution of concentration 9×10^{10} particles/cm^3. The temperature at the center of the laser excitation area has been estimated for laser excitation of a gold colloidal droplet[7,9] (eq 1) or for a spherical region with randomly distributed nanoparticle heat sources[8] (eq 2). Equation 2 gives the temperature increase of a heater with a characteristic size R_{heat} and it is valid relatively far from the cylinder surface. In eqs 1 and 2, C_{abs} is the absorption cross section of a 40 nm gold nanoparticle immersed in water (2.8×10^{-15} m^2), I (W/m^2) is the intensity of the excitation laser (Power (W) $\times$ 1.8×10^7 m^{-2}), R_{NP} is the gold nanoparticle radius (20 nm), η_{NP} is the nanoparticle concentration (9×10^{10} particles/cm^3), l_{opt} is the optical path length (1.649 mm), R_{beam} is the radius of the optical beam (0.136 mm).[7,9] Theory (eq 1) generally underestimates the temperature for the 100 mW excitation, shown as the large blue point in Figure 7, while theory from a spherical heated region (eq 2) overestimates the temperature (shown as the large red point). The thermal profile away from the cylinder of laser excitation has been previously calculated.[7] The damping of the temperature away from the excitation region has an exponential decay but at a larger damping rate than the experimental thermal profiles shown in Figure 7B. Theory overestimates the damping of the temperature profile away from the excitation region because thermal diffusion due to convection is neglected.

$$\Delta T \approx \frac{C_{abs} I \eta_{NP} R_{beam}^2 \log_e(l_{opt}/R_{beam})}{2k_w} \quad (1)$$

$$\Delta T_{global} = \frac{C_{abs} I \eta_{NP} {R_{heat}}^2}{2k_w} \quad (2)$$

Convection within the liquid is probed by measuring the temperature distribution within the optically stimulated liquid as the laser is moved from the bottom to top of the sample cell. The laser power is held constant at 1.25 W and the thermal profiles are shown in Figure 8. In the diagram, shown in the far left of Figure 8A, the laser is excited at the positions labeled as 1−5 and are color coded to the temperature profiles shown in Figure 8B. The direction of heat flow in the liquid is shown as dotted lines in Figure 8B when the sample is heated at laser position 3. The temperature profiles within the liquid at different laser positions are shown in Figure 8C. The color coded arrows show the position of the laser excitation. When the sample is excited in the middle of the sample cell (laser position 3, red data), the temperature in the liquid 2 mm above the laser spot is higher than the temperature at the laser spot. Conversely, the temperature in the liquid 2 mm below the laser spot is cooler than the temperature at the laser spot. This trend is observed for all the laser positions except for position 5 where the sample

is excited near the bottom of the sample cell. We believe that this effect is consistent with fluid motion through convection consistent with our observation from micrometer sized silica beads in laser excited gold colloidal droplets.[19]

Collective Heating Mechanism in Solution and Other Systems. In the nanoparticle solution experiment, the mechanism of heating is collective and this mechanism is amazingly efficient. In the mechanism, heat fluxes from a large ensemble of small nanoparticles add up and the resultant temperature of water becomes a few orders of magnitude larger than the temperature that can be created by a single nanoparticle (NP). We now illustrate this mechanism for the model of light−heated cylinder submerged in water[7,9] for the temperatures below the boiling point. When the temperature is above the boiling point, the phase transformation takes place, the temperature within the boiling area stays constant at 100 °C, and the estimates given below are no longer applied. The heater in our model is a cylinder with the length l_{opt} and the radius R_{beam}. Then, the ratio between the collective temperature in the center of a heated cylinder and the single-nanoparticle temperature is written as[7,9]

$$A = \frac{\Delta T_{collective}}{\Delta T_{surface\ of\ single\ particle}} \approx R_{NP}\eta_{NP}S_{beam}2\log_e(l_{opt}/R_{beam}) = N_{NP,tot}\frac{R_{NP}}{l_{opt}}2\log_e(l_{opt}/R_{beam}) \quad (3)$$

where S_{beam} is the beam cross-sectional area and $N_{NP,tot}$ is the total number of NPs inside the beam cylinder. The temperature increase at the surface of single, isolated NP is given by the standard equation: $\Delta T_{surface\ of\ single\ particle} = C_{abs}I/4\pi k_w$. For a 3D compact nanoparticle heater, this equation looks simpler: $\Delta T_{collective}/\Delta T_{surface\ of\ single\ particle} \approx N_{NP,tot}R_{NP}/R_{heater}$, where R_{heater} is the size of a NP complex. The transition between the single-particle and collective regimes of heating depends on the parameter A given by eq 3. For a solution with a high NP density, the parameter $A \gg 1$ and the collective heating is realized. In the opposite case of small NP densities, the parameter $A \ll 1$, the local temperature increase at the NP surface dominates and the collective effect can be neglected. For the case of the solution experiment shown in Figures 7, the collective parameter is a large number, $A \sim 520$, since the NP density is high ($\eta_{NP} = 9 \times 10^{10}$ cm^{-3}). This is the regime when the heating is very efficient due to its collective character. For example, at the 100mW-power, the estimated collective temperature increase in the middle of the heated cylinder is ~17 °C, whereas the single NP temperature increase is only 0.04 °C. The total number of NPs involved in the collective heating in Figure 7 is $\sim 8 \times 10^6$. For the geometry of the experiment in Figure 8, the transition between two regimes of heating occurs at $\eta_{NP} = 1.7 \times 10^8$ cm^{-3} when $A = 1$.

Vapor-Nucleation Picture and the Rate of Bubble Creation for a Single Nanowrench and for the Nanoparticle Solution. The vapor-nucleation scenario is based on the nucleation center where the formation of a bubble starts (Figure 9a).[5] This can be a small air bubble or other object favoring the steam nucleation. Then, the volume of the superheated liquid is an important parameter for the case of the single nanowrench experiment because the number of nucleation centers found in the superheated volume will determine the number of bubbles formed. Such volume can be roughly estimated assuming that a nanowrench is a compact spherical object. Then, the volume of the superheated water, in which the temperature varies in the interval 100 °C < T < $T_{surface}$, is calculated as: $R_{superheated} = C_{abs,nanowrench}I/4\pi(100\ °C - T_{ambient})$, where $= (k_w + k_{substrate})/2$ is the averaged thermal conductivity of the system. Figure 9c shows the estimated volume of overheated liquid around of the nanowrench for the interval of intensities that provides the temperature interval for nanoparticle surface temperature 100 °C < $T_{surface}$ < 305 °C, where 305 °C is the spinodal decomposition temperature of water.[14] Above the spinodal decomposition temperature a nucleation center is not needed for bubble formation while below the spinodal decomposition temperature a nucleation center is needed. Therefore, we can assume that the rate of formation of bubbles is proportional to an average number of nucleation centers within the superheated volume:

$$\mathrm{Rate}_{bubble} = \frac{1}{\Delta t_{bubble}} \sim V_{superheated}c_{centers} = \frac{1}{2}\frac{4\pi}{3}(R^3_{superheated} - R^3_{eff,\ nanowrench})c_{centers}$$

where $c_{centers}$ is the concentration of nucleation centers, Δt_{bubble} is the time interval between two consecutive creations of bubbles, and $R_{eff,nanowrench}$ is the effective radius of the nanowrench. When we look at the setting with boiling of water using the nanoparticle solution and the laser beam (Figure 6), we see really a striking difference in the effect and in the volume of water having the boiling temperature 100 °C. Since the system is in the regime of phase transformation and it (the light beam cylinder) is macroscopic, the temperature of the boiling water should be taken as 100 °C. Then, the volume of the boiling water is approximately equal to the volume of the beam. This boiling volume is $V_{boiling} \sim 0.095$ mm^3. In the case of the surface nanostructure (nanowrench) experiment, the estimated volume of the superheated water is dramatically small, $V_{superheated} \sim 10^{-10}$ mm^3, and therefore, the probability of bubble creation is dramatically low. In our experiments, bubbles from a single nanowrench can

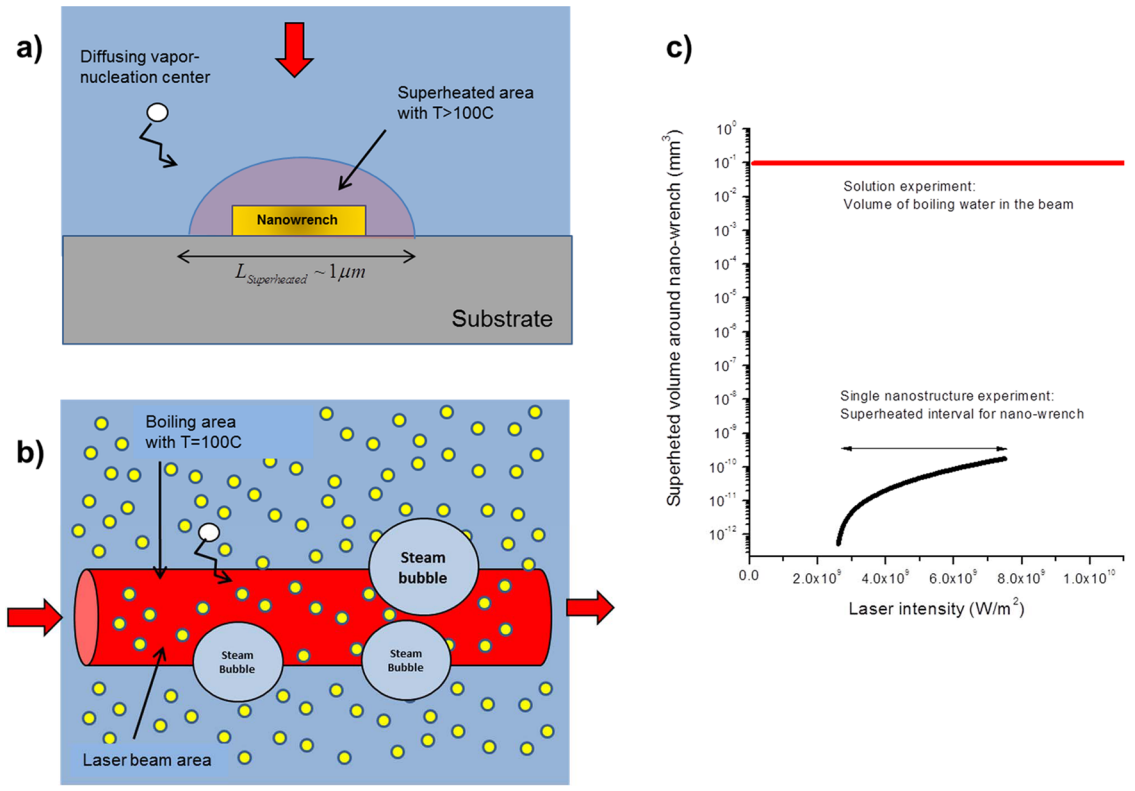

Figure 9. (a and b) Schematic illustrations of physical processes involved in this study. Panel a illustrates the experiment with an optically excited nanowrench submerged into water, whereas panel b describes the nanoparticle solution experiment. (c) Calculated volume of the superheated water in the single nanowrench experiment (black curve) and the volume of boiling region in the case of the solution experiment (red line). The superheated water volume is shown only for the corresponding interval of intensities when the system is above the boiling point but below the spinodal.

be observed, but they are very rare events. While for the nanoparticle solution the boiling is very active and bubbles are created frequently using relatively small laser intensities, $I \sim 10^7$ W/m^2. This can be explained considering the ratio $V_{superheated}/V_{boiling} \sim 10^{-9}$. In other words, the volume for steam nucleation in the single nanowrench experiment 9 orders of magnitude smaller than that for the solution experiment! This simple volume consideration explains the striking difference of the two cases and a long waiting time for the observation of a bubble in the single nanowrench experiment.

Contrast between Phase Transformation for Single Plasmonic Particle (Nanowrench) and 3D Nanoparticle Solution. A single nanoscale hot spot created at a solid/liquid interface (*e.g.*, a nanowrench in our study) nucleates vapor bubbles rarely below the spinodal decomposition temperature. The laser intensity needed to drive the temperature of the gold embedded nanoheater is given by the heat transfer equation.[7,9,13−15] At the spinodal decomposition temperature, the variation in the temperature increases because of instabilities created by scattering of the laser due to critical opalescence.[14] This behavior is supported by theory where, even in a colloidal gold nanoparticle solution, if the nanoparticle density is sufficiently reduced and the laser intensity increased, large temperature spikes around the nanoheater is expected with little change in the ambient temperature.[7,20]

Colloidal gold nanoparticle solutions with higher densities, where collective heating effects dominate, have very different phase transition properties. First, there is an amplification of the temperature input to the surroundings, due to collective heating effects, that scales with the number of nanoheaters excited.[8,9] This amplification can be extremely high, $\sim 10^7$, causing a similar change in the temperature of the surrounding liquid with much lower laser intensities than exciting single nanoparticle heaters. Also, a macroscopic region of the solution temperature is increased, not just a local region around the nanoheater. The large volume liquid can be driven at relatively low laser intensities to the boiling point of the liquid where vapor nucleation occurs with high efficiency and the solution does not superheat.

Finally, it is possible to build three-dimensional clusters of oxide nanoparticles with multiple small (5 nm) gold nanoparticles that have a similar spacing as nanoparticles in colloidal solutions. These clusters absorb light and through collective heating effects raise the water temperature to the boiling point where vapor nucleation happens effectively. We are currently trying to understand how length scales and structural organization of nanoheaters at solid/liquid interfaces affect superheating and vapor nucleation.

CONCLUSIONS

The heating effect and phase transformation properties of water are studied for a single nanowrench at a solid/liquid interface and an ensemble of gold nanoparticles in solution. The temperature of the optically excited nanowrench was measured as a function of time for different laser intensities. The thermal properties of the nanowrench show a linear increase in temperature with increase in laser intensity until a temperature of 580 ± 20 K where the properties change. The temperature increase in no longer linear with laser intensity and the variation in temperature increases dramatically at this demarcation point. The temperature of 580 K is assigned as the spinodal decomposition temperature of water where the metastable liquid becomes unstable. Vapor nucleation below the spinodal decomposition temperature and above the boiling point is observed but only as a rare event. These results are contrasted to an ensemble of optically excited gold nanoparticles in solution where vapor formation at the boiling point is the norm. The ambient liquid temperature is raised to the boiling point by collective heating effects of an ensemble of excited nanoparticles where boiling occurs within the solution and not necessarily at the surface of the nanoparticles.

MATERIALS AND METHODS

Optical Measurements of Temperature. The optical measurements and characterization of the thermal sensor film has been described in detail previously.[15] We use a thin film (~270 nm thick) of $Al_{0.94}Ga_{0.06}N$ embedded with Er^{3+} ions on a silicon substrate as a thermal sensor film by measuring the relative photoluminescent intensities of the $^2H_{11/2} \rightarrow {}^4I_{15/2}$ and the $^4S_{3/2} \rightarrow {}^4I_{15/2}$ energy transitions of the Er^{3+} ions. These intensities have been shown to be temperature dependent[21,22] and are related by a Boltzmann factor ($\exp(-\Delta E/kT)$) where ΔE is the energy difference between the two levels, k is the Boltzmann constant, and T is the absolute temperature.

The optical measurements were made with a WITec α-SNOM300s. A CW 532 nm wavelength Nd:YAG laser with adjustable power is focused with a Nikon 60× water immersion lens onto the thin film thermal sensor. The emission from the thermal sensor is collected with the same lens and sent to the CCD spectrograph with a collection fiber. A survey spectral image was first taken to locate the particle. Once the position of the nanostructure was located, a background time spectrum was taken with laser excitation over a period of time while focused on the region with no nanostructure. A time spectrum was then taken while focused on the nanostructure for a period of time. The temperature spectrum was then constructed from the photoluminescence spectrum collected for both the background and the nanostructure excitation. The temperature difference spectrum was generated by taking the difference between the time temperature spectrum for sample and background.

Fabrication of Gold Nanowrenches. Gold nanowrenches are fabricated using conventional e-beam lithography with lift-off. The height of the nanowrench is 65 nm measured with a Nanoscope IIIA Multimode AFM. The SEM image of a pair of nanowrenches is shown in Figure 1. The nanowrench has a standard width of 400 nm and a length of 700 nm. The width and length was measured with a JEOL JSM-5300 Scanning Electron Microscope. A single layer of around 100 nm of poly(methyl methacrylate) (PMMA) (950K A4 PMMA in Anisole) positive resist was spin coated onto the $Al_{0.94}Ga_{0.06}N:Er^{3+}$ thin film on Si. The PMMA was filtered through a 0.2 um frit to remove bubbles. The PMMA coated samples were baked on a hot plate at 205 °C for 5 min. After baking step, electron beam lithography (~50 kV) was performed to draw the desired pattern with a resolution of ~10 nm. The samples were then developed with MIBK:IPA = 1:3 (volume) for 30 s, rinsed/cleaned with IPA, and dried with N_2. A thin adhesion layer of Ti (5 nm) was first deposited then followed by a thicker (60 nm) layer of Au using DC sputtering. The residual layer was removed with a warm (60 °C) acetone bath.

Temperature Measurements of Optically Excited Colloidal Gold Nanoparticles. The gold colloid solution (British Biocell International) was degassed with helium, transferred to a precut capillary tube, and aligned with a 532 nm laser. The colloidal solution is first heated to drive out the remaining helium gas. A thermocouple is then lowered into the capillary and positioned at an intended distance away from the laser excitation region. Data collection was then initiated at a single distance with known laser intensity. During data collection, the temperature of the solution rose until a steady state temperature was achieved. Once steady state was observed, the laser beam was blocked and the laser intensity changed for the next measurement by rotating a variable neutral density filter. The laser power was checked with a power meter and the position of the laser beam relative to the top of the liquid was recorded. A DVD recorder captured a movie of the laser heating experiment and Image J was used to extract distances between the thermocouple, the laser beam spot, and the top of the liquid for each data collection measurement.

Temperature Measurements Probing Convection of the Liquid during Laser Excitation of a Colloidal Nanoparticle Solution. A sample cell is constructed using a thick double sided tape in between two glass slides. The sample cell is constructed so that multiple temperature measurements can be made simultaneously. The cell dimensions (4 mm wide × 1 mm thick × 12 mm tall) are larger than the diameter of the capillary tube (2 mm). Along each side of the cell is an array of thermocouples used to measure temperature simultaneously at different points in the cell. The thermocouples that are directly across from each other are wired in parallel so that an average temperature is measured between those two probes. A 40 nm gold nanoparticle solution poured into the chamber and irradiated at 1.25 W. The temperature from each paired thermocouple is recorded at one laser spot position; the laser spot is then moved down the sample cell and the thermocouple temperatures are measured again.

Conflict of Interest: The authors declare no competing financial interest.

Acknowledgment. The authors thank Ohio State University center of Nanofabrication for their help in e-beam fabrication of the nanostructures and the Condensed Matter and Surface Science Program at Ohio University.

Supporting Information Available: Additional information showing boiling of colloidal solution with 532 nm laser excitation. This material is available free of charge *via* the Internet at http://pubs.acs.org.

REFERENCES AND NOTES

1. Reddy, K. S.; Kumar, K. R.; Devaraj, V. A. Feasibility Analysis of Megawatt Scale Solar Thermal Power Plants. *J. Renewable Sustainable Energy* **2012**, *4*, 063111–23.
2. Neumann, O.; Urban, A. S.; Day, J.; Lal, S.; Nordlander, P.; Halas, N. J. Solar Vapor Generation Enabled by Nanoparticles. *ACS Nano* **2013**, *7*, 42–49.
3. Neumann, O.; Feronti, C.; Neumann, A. D.; Dong, A.; Schell, K.; Lu, B.; Kim, E.; Quinn, M.; Thompson, S.; Grady, N.; *et al.*

Compact Solar Autoclave Based on Steam Generation Using Broadband Light-Harvesting Nanoparticles. *Proc. Natl. Acad. Sci. U. S. A.* **2013**, *110*, 11677–11681.
4. Fang, Z.; Zhen, Y.-R.; Neumann, O.; Polman, A.; Garcia de Abajo, F. J.; Nordlander, P.; Halas, N. J. Evolution of Light-Induced Vapor Generation at a Liquid-Immersed Metallic Nanoparticle. *Nano Lett.* **2013**, *13*, 1736–1742.
5. Carey, V. P. *Liquid-Vapor Phase-Change Phenomena*, 2nd ed.; Taylor and Francis: New York, 2008.
6. Witharana, S.; Phillips, B.; Strobel, S.; Kim, H. D.; McKrell, T.; Chang, J. B.; Buongiorno, J.; Berggren, K. K.; Chen, L.; Ding, Y. Bubble Nucleation on Nano- to Micro-Size Cavities and Posts: An Experimental Validation of Classical Theory. *J. Appl. Phys.* **2012**, *112*, 064904–5.
7. Richardson, H. H.; Carlson, M. T.; Tandler, P. J.; Hernandez, P.; Govorov, A. O. Experimental and Theoretical Studies of Light-to-Heat Conversion and Collective Heating Effects in Metal Nanoparticle Solutions. *Nano Lett.* **2009**, *9*, 1139–1146.
8. Keblinski, P.; Cahill, D. G.; Bodapati, A.; Sullivan, C. R.; Taton, T. A. Limits of Localized Heating by Electromagnetically Excited Nanoparticles. *J. Appl. Phys.* **2006**, *100*, 054305–5.
9. Govorov, A. O.; Zhang, W.; Skeini, T.; Richardson, H.; Lee, J.; Kotov, N. A. Gold Nanoparticle Ensembles as Heaters and Actuators: Melting and Collective Plasmon Resonances. *Nanoscale Res. Lett.* **2006**, *1*, 84–90.
10. Huehn, D.; Govorov, A.; Gil, P. R.; Parak, W. J. Photostimulated Au Nanoheaters in Polymer and Biological Media: Characterization of Mechanical Destruction and Boiling. *Adv. Funct. Mater.* **2012**, *22*, 294–303.
11. Stehr, J.; Hrelescu, C.; Sperling, R. A.; Raschke, G.; Wunderlich, M.; Nichtl, A.; Heindl, D.; Kurzinger, K.; Parak, W. J.; Klar, T. A.; *et al.* Gold Nanostoves for Microsecond DNA Melting Analysis. *Nano Lett.* **2008**, *8*, 619–623.
12. Baffou, G.; Berto, P.; Urena, E. B.; Quidant, R.; Monneret, S.; Polleux, J.; Rigneault, H. Photoinduced Heating of Nanoparticle Arrays. *ACS Nano* **2013**, *7*, 6478–6488.
13. Richardson, H. H.; Hickman, Z. N.; Govorov, A. O.; Thomas, A. C.; Zhang, W.; Kordesch, M. E. Thermooptical Properties of Gold Nanoparticles Embedded in Ice: Characterization of Heat Generation and Melting. *Nano Lett.* **2006**, *6*, 783–788.
14. Carlson, M. T.; Green, A. J.; Richardson, H. H. Superheating Water by Cw Excitation of Gold Nanodots. *Nano Lett.* **2012**, *12*, 1534–1537.
15. Carlson, M. T.; Khan, A.; Richardson, H. H. Local Temperature Determination of Optically Excited Nanoparticles and Nanodots. *Nano Lett.* **2011**, *11*, 1061–1069.
16. Green, A. J.; Alaulamie, A. A.; Baral, S.; Richardson, H. H. Ultrasensitive Molecular Detection Using Thermal Conductance of a Hydrophobic Gold-Water Interface. *Nano Lett.* **2013**, *13*, 4142–4147.
17. Vogel, A.; Venugopalan, V. Mechanisms of Pulsed Laser Ablation of Biological Tissues. *Chem. Rev.* **2003**, *103*, 577–644.
18. Apfel, R. E. Water Superheated to 279.5 °C at Atmospheric-Pressure. *Nat. Phys. Sci.* **1972**, *238*, 63–64.
19. Carlson, M. T.; Barton, T. S.; Tandler, P. J.; Richardson, H. H.; Govorov, A. O. Thermal Effects of Colloidal Suspensions of Au Nanoparticles. *Mater. Res. Soc. Symp. Proc.* **2009**, *1172*, T05–08.
20. Govorov, A. O.; Richardson, H. H. Generating Heat with Metal Nanoparticles. *Nano Today* **2007**, *2*, 30–38.
21. Gurumurugan, K.; Chen, H.; Harp, G. R.; Jadwisienczak, W. M.; Lozykowski, H. J. Visible Cathodoluminescence of Er-Doped Amorphous Aln Thin Films. *Appl. Phys. Lett.* **1999**, *74*, 3008–3010.
22. Garter, M. J.; Steckl, A. J. Temperature Behavior of Visible and Infrared Electroluminescent Devices Fabricated on Erbium-Doped Gan. *IEEE Trans. Elect. Dev* **2002**, *49*, 48–54.